High-Precision Calibration and Error Estimation of RLG SINS

Yikun Geng[1,2] and Xiyuan Chen[1,2(✉)]

[1] Key Laboratory of Micro-Inertial Instrument and Advanced Navigation Technology Ministry of Education, Southeast University, Nanjing 210096, China
chxiyuan@seu.edu.cn

[2] School of Instrument Science and Engineering, Southeast University, Nanjing 210096, China

Abstract. Since sensor errors limit navigation accuracy in ring laser gyroscope strapdown inertial navigation system (RLG SINS), the calibration of the error parameters is usually a key technology of SINS. This paper mainly studies the error estimation and high-precision calibration of RLG SINS under both static and small-angle swing bases using systematic calibration method. In this paper, firstly, based on the analysis of the error source, the error models of the quartz flexible accelerometers and laser gyroscopes are established. Meanwhile, according to the basic principles of SINS, the error equations of SINS in navigation coordinate system are derived. Then, this paper studies systematic calibration method. In this part, a multi position rotation error excitation method is introduced and a 33-dimensional Kalman filter is designed for the estimation of the error parameters. Finally, the simulation experiments for the error calibration of the inertial sensors under both static and small-angle swing conditions are performed to verify the effectiveness of this systematic calibration method. This method performs well in the simulation experiments and has its value in the online calibration of slight swing conditions, such as ship mooring state and the missile launcher swing state.

Keywords: SINS · Systematic calibration · Error parameter estimation

1 Introduction

The SINS uses three gyroscopes and three accelerometers to measure the angular velocity and acceleration respectively and subsequently calculate the attitude, velocity and position information continuously based on the dead reckoning principle [1]. Therefore, the inertial navigation, a fully autonomous navigation technology, has the characteristic of accumulating positioning errors over time which leads to the result that the error parameter calibration of SINS has great influences on the navigation accuracy. The main calibration methods mainly include discrete calibration and systematic calibration. Among them, systematic calibration establishes the relationship between navigation errors and inertial sensor error parameters, which usually uses navigation errors as the quantitative measurement to estimate the error parameters. This method can calibrate all error parameters simultaneously through the calculation and allows the

© ICST Institute for Computer Sciences, Social Informatics and Telecommunications Engineering 2021
Published by Springer Nature Switzerland AG 2021. All Rights Reserved
W. Fu et al. (Eds.): ICMTEL 2021, LNICST 387, pp. 460–469, 2021.
https://doi.org/10.1007/978-3-030-82562-1_44

accurate attitude of the inertial measurement unit (IMU) unknown, which is therefore also a good online calibration method due to the reduced dependence on the accuracy of the turntable compared to discrete calibration [12–15]. There are lots of studies on self-calibration to establish a proper error model to estimate one or more error parameters of IMU, such as the bias, the scale factor errors, the installation errors and the non-linear errors of gyroscopes and accelerometers. Besides, the designs of error excitation scheme and the observability analysis, the filtering method and signal processing have all been extensively studied worldwide [2–11].

In this essay, a method to perform systematic calibration under both static and small-angle swing bases is developed, which uses the designed multi position rotation scheme to excite the inertial sensor errors, including the bias, the scale factor errors and the misalignments of both two types of the sensors and the quadratic errors of accelerometers. In the simulation experiments, this method performs well under both static and small-angle swing bases, which makes it of certain reference value in the online calibration under the ship mooring state and the missile launcher swing state.

This paper is organized as follows. In Sect. 2, based on the analysis of error source, the error models of the accelerometers and laser gyroscopes are introduced and subsequently the SINS error equations are derived. In Sect. 3, the overall systematic calibration process suitable for both static and small-angle swing bases is introduced firstly and then the multi position rotation error excitation scheme and the Kalman filter used in this article are given. In Sect. 4, the simulation experiments are performed. The results of systematic calibration simulation experiments under both static and small-angle swing bases are given, including the error parameters estimated results and the compensation performance analysis. Section 5 is the conclusion.

2 Error Model

2.1 Sensor Error Model

The inertial sensors of the RLG SINS are composed of three laser gyroscopes and three quartz flexible accelerometers. In the traditional IMU error model, several of the following errors are usually considered, including the bias, the scale factor errors and the misalignments of gyroscopes and accelerometers. In this article, considering the small-angle swing bases, the non-linear errors of the accelerometers may have a great impact on the accuracy of the inertial navigation. Therefore, in order to achieve high-precision calibration under both static and small-angle swing bases, on the basis of the traditional inertial sensor error models, the quadratic errors of accelerometers are added into the accelerometer error model. The formulas of the simplified error model [10] of the gyroscopes and the accelerometers are expressed respectively as follows:

$$\begin{bmatrix} \varepsilon_x \\ \varepsilon_y \\ \varepsilon_z \end{bmatrix} = \begin{bmatrix} B_{gx} \\ B_{gy} \\ B_{gz} \end{bmatrix} + \left(\begin{bmatrix} K_{gx} & 0 & 0 \\ 0 & K_{gy} & 0 \\ 0 & 0 & K_{gz} \end{bmatrix} + \begin{bmatrix} 0 & M_{gxy} & M_{gxz} \\ M_{gyx} & 0 & M_{gyz} \\ M_{gzx} & M_{gzy} & 0 \end{bmatrix} \right) \begin{bmatrix} \omega_x^b \\ \omega_y^b \\ \omega_z^b \end{bmatrix} \quad (1)$$

$$\begin{bmatrix} \delta f_x^b \\ \delta f_y^b \\ \delta f_z^b \end{bmatrix} = \begin{bmatrix} B_{ax} \\ B_{ay} \\ B_{az} \end{bmatrix} + \left(\begin{bmatrix} K_{ax} & 0 & 0 \\ 0 & K_{ay} & 0 \\ 0 & 0 & K_{az} \end{bmatrix} + \begin{bmatrix} 0 & M_{axy} & M_{axz} \\ M_{ayx} & 0 & M_{ayz} \\ M_{azx} & M_{azy} & 0 \end{bmatrix} \right) \begin{bmatrix} f_x^b \\ f_y^b \\ f_z^b \end{bmatrix} + \begin{bmatrix} D_{ax} \\ D_{ay} \\ D_{az} \end{bmatrix} \begin{bmatrix} f_x^{b^2} \\ f_y^{b^2} \\ f_z^{b^2} \end{bmatrix} \tag{2}$$

where ε_i is the total angular velocity error in the i direction of the gyroscopes; ω_i^b is the angular velocity on IMU axes; δf_i^b is the specific force error on IMU axes of the accelerometers; f_i^b is the specific force; $f_x^{b^2}$ is the quadratic term of the specific force; B_{gi} and B_{ai} represent the bias of gyroscopes and accelerometers respectively; K_{gi} and K_{ai} are the scale factor errors of gyroscopes and accelerometers respectively; M_{gij} and M_{aij} represent the non-orthogonal installation errors; the IMU axes are defined by the sensitive axes of the accelerometers and therefore $M_{axy}=M_{axz}=M_{ayz}=0$; D_{ai}. represents the quadratic error of the accelerometers in the i direction.

Formula (1) uses the sum of the bias of gyroscopes and the product of the measured angular velocities and the error matrix to express the angular velocity errors of gyroscopes. Similarly, formula (2) uses the sum of the bias of accelerometers, the product of the measured specific forces and the first-order error matrix, and the product of the quadratic terms of the specific forces and quadratic error matrix to express the specific force errors of the accelerometers. These two formulas of the inertial sensor model establish the relationship between the inertial sensor errors and the measurement errors of the inertial sensors.

2.2 SINS Error Model

Since there are errors between the ideal navigation coordinate system and the actual navigation coordinate system, in order to reflect the changes of the error angles between these two coordinate systems, the attitude error equations of SINS [11] are derived and established as follows:

$$\begin{cases} \delta\dot{\varphi}_x = -\frac{\delta V_N}{R_e} + \left(\omega_{ie}\sin L + \frac{V_E}{R_e}\tan L\right)\delta\varphi_N - \left(\omega_{ie}\cos L + \frac{V_E}{R_e}\right)\delta\varphi_U + \varepsilon_x^n \\ \delta\dot{\varphi}_y = \frac{\delta V_E}{R_e} - \left(\omega_{ie}\sin L + \frac{V_E}{R_e}\tan L\right)\delta\varphi_E - \frac{V_N}{R_e}\delta\varphi_U + \varepsilon_y^n \\ \delta\dot{\varphi}_z = \frac{\delta V_E}{R_e}\tan L + \left(\omega_{ie}\cos L + \frac{V_E}{R_e}\right)\delta\varphi_E + \frac{V_N}{R_e}\delta\varphi_N + \varepsilon_z^n \end{cases} \tag{3}$$

where R_e is the radius of the earth; L is the latitude of the IMU; V_I is the speed in navigation coordinate system; ω_{ie} is earth rotation velocity.

Besides, there are also errors between the ideal speeds and the speeds obtained by calculation. The speed error equations of SINS [11] are shown as follows:

$$\begin{cases} \delta\dot{v}_x^n = \frac{V_N}{R_e}\tan L\cdot\delta V_E + \left(2\omega_{ie}\sin L + \frac{V_E}{R_e}\tan L\right)\delta V_N - \left(2\omega_{ie}\cos L + \frac{V_E}{R_e}\right)\delta V_U + g\cdot\delta\varphi_N + \delta f_x^n \\ \delta\dot{v}_y^n = \left(-2\omega_{ie}\sin L + \frac{2V_E}{R_e}\tan L\right)\delta V_E - \frac{V_U}{R_e}\delta V_N - \frac{V_N}{R_e}\delta V_U - g\cdot\delta\varphi_E + \delta f_y^n \\ \delta\dot{v}_z^n = \left(2\omega_{ie}\cos L + \frac{2V_E}{R_e}\right)\delta V_E + \frac{2V_U}{R_e}\delta V_N + \delta f_z^n \end{cases} \tag{4}$$

The formula (3) and the formula (4) of the SINS error model establish the relationship between the navigation errors and the measurement errors of the inertial sensor. Combining formula (1) and formula (2), the relationship between the navigation errors and the inertial sensor errors is finally established. In this way, navigation errors can be used as the quantitative measurement to estimate the inertial sensor error parameters to perform systematic calibration.

3 Systematic Calibration Method

3.1 Systematic Calibration Process

In order to study the high-precision calibration and error estimation of RLG SINS under both static and small-angle swing bases, the systematic calibration method is used to calibrate the inertial sensor errors by using navigation errors as the quantitative measurement. The systematic calibration process flow chart is shown in Fig. 1. The overall systematic calibration process steps are as follows:

Step 1. Collect the simulated output signals of the IMU which rotates according to the multi position error excitation scheme.

Step 2. Calculate the navigation speed errors in RLG SINS.

Step 3. Input the speed errors as the quantity measurement into the Kalman filter.

Step 4. Continue Kalman filtering until all the collected data are traversed.

Step 5. Feedback the estimated error parameters to compensate the output signals of inertial sensors.

Step 6. Repeat step 2–step 5 until the preset number of iterations is reached.

Step 7. Output the final calibration results of the estimated error parameters.

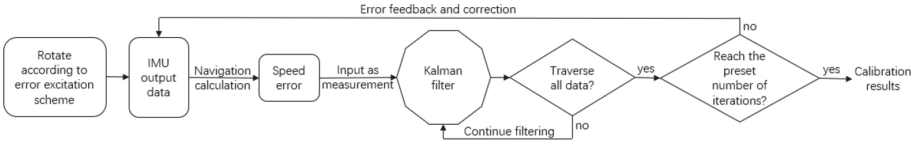

Fig. 1. Systematic calibration process flow chart. Kalman filter is used to estimate the error parameters and the estimation results are used to compensate the original IMU output data.

3.2 Rotation Error Excitation Scheme

Traditional offline calibration methods generally use proper rotation schemes under the static base in the laboratory to excite errors. Traditional online calibration methods, such as [16] and [17], generally design motion paths adapting to the application environment for the IMU by using actions such as straight going at a constant speed, rolling, turning and pitching to complete the excitation of the errors. In this article, however, due to the limitation of the application condition, the movement actions performed by other online calibration methods cannot be realized. Therefore, the rotation error excitation method is used, while the applicability under both static and small-angle swing bases should be taken into consideration in the subsequent simulation experiments.

According to the multi position rotation error excitation method mentioned in reference [8], a trajectory generator is compiled to simulate the rotation of IMU to excite the inertial sensor errors under both static and small-angle swing bases. At the end of the whole process, the IMU has rotated 720° around each axis, and returned to the initial posture, which helps to observe the error parameters. The multi position rotation error excitation scheme is shown in Fig. 2.

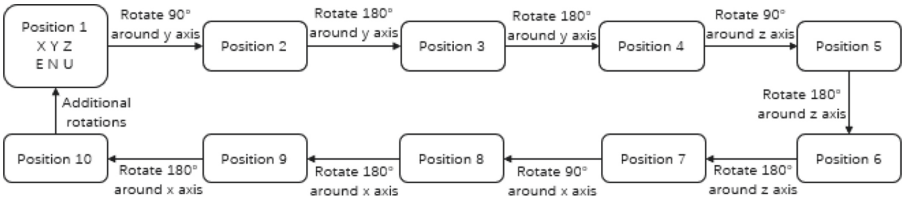

Fig. 2. The multi position rotation error excitation scheme. The rotation speed is 10 °/s. The IMU stays stationary at each position for 10 min to fully stimulate the errors. In the additional rotations, the IMU rotates 90 ° for three times around each of the x, y, and z axes respectively and also stays stationary for a period of time at each position.

3.3 Kalman Filter

In order to separate the calibration error parameters, a suitable Kalman filter needs to be designed. In this article, the Kalman filter uses error model to establish the state equation [8, 15], where Gaussian white noise model is used as the sensor noise model. The system error differential equation is expressed as follows:

$$\dot{X}(t)=F(t)X(t)+G(t)W(t) \tag{5}$$

where X(t) is expressed as follow:

$X(t)=[\delta\varphi_x, \delta\varphi_y, \delta\varphi_z, \delta v_x^n, \delta v_y^n, \delta v_z^n, B_{gx}, B_{gy}, B_{gz}, B_{ax}, B_{ay}, B_{az}, K_{gx}, M_{gyx}, M_{gzx}, M_{gxy}, K_{gy}, M_{gzy}, M_{gxz}, M_{gyz}, K_{gz}, K_{ax}, M_{ayx}, M_{azx}, M_{axy}, K_{ay}, M_{azy}, M_{axz}, M_{ayz}, K_{az}, D_{ax}, D_{ay}, D_{az}]$

In (5), W(t) is the measurement noise of Gaussian white noise model, W(t)~N (0, Q) and $W(t) = [\delta\omega\ \delta f]^T$, where gyroscope measurement noise $\delta\omega = \left[\delta\omega_x\ \delta\omega_y\ \delta\omega_z\right]^T$; accelerometer measurement noise $\delta f = \left[\delta f_x\ \delta f_y\ \delta f_z\right]^T$. G(t) is the system noise output matrix and $G(t) = \begin{bmatrix} -C_b^n & 0_{3\times3} \\ 0_{3\times3} & C_b^n \\ 0_{27\times3} & 0_{27\times3} \end{bmatrix}$. F(t), the system state matrix, is obtained by calculating velocity error equations and attitude error equations and is expressed as follows:

$$F(t) = \begin{bmatrix} -\left[\omega_{in}^n\times\right] & F_{12} & -C_b^n & 0_{3\times3} & F_{15} & 0_{3\times9} & 0_{3\times3} \\ \left[f^n\times\right] & F_{22} & 0_{3\times3} & C_b^n & 0_{3\times9} & F_{26} & F_{27} \\ 0_{27\times3} & 0_{27\times3} & 0_{27\times3} & 0_{27\times3} & 0_{27\times9} & 0_{27\times9} & 0_{27\times3} \end{bmatrix} \tag{6}$$

$$\text{where } F_{12} = \begin{bmatrix} 0 & -\frac{1}{R_M+h} & 0 \\ \frac{1}{R_N+h} & 0 & 0 \\ \frac{tanL}{R_N+h} & 0 & 0 \end{bmatrix}, F_{27} = C_b^n \begin{bmatrix} f_x^{b^2} & 0 & 0 \\ 0 & f_y^{b^2} & 0 \\ 0 & 0 & f_z^{b^2} \end{bmatrix},$$

$$F_{22} = \begin{bmatrix} \frac{v_y tanL - v_z}{R_N+h} & \frac{v_x}{R_N+h} + 2\omega_{ie} sinL & -\frac{v_x}{R_N+h} - 2\omega_{ie} cosL \\ \frac{-2v_x tanL}{R_N+h} 2\omega_{ie} sinL & -\frac{v_z}{R_M+h} & -\frac{v_y}{R_M+h} \\ \frac{2v_x}{R_N+h} + 2\omega_{ie} cosL & \frac{2v_y}{R_N+h} & 0 \end{bmatrix},$$

$$F_{26} = \begin{bmatrix} C_b^n \cdot f_x^b & C_b^n \cdot f_y^b & C_b^n \cdot f_z^b \end{bmatrix}, \; F_{15} = \begin{bmatrix} -C_b^n \cdot \omega_x^b & -C_b^n \cdot \omega_y^b & -C_b^n \cdot \omega_z^b \end{bmatrix}.$$

The observation equation takes velocity errors as the observation and is expressed as follow:

$$Z_v(t) = H_v(t)X(t) + v_v(t) \tag{7}$$

where the observation matrix $H_v(t) = \begin{bmatrix} 0_{3\times3} & I_{3\times3} & 0_{3\times27} \end{bmatrix}$; the system observation noise is of Gaussian white noise model: $v_v(t) \sim N(0, R)$.

4 Calibration Simulation Experiments

In this article, the calibration simulation experiments under both static base and small-angle swing base are performed. The trajectory simulation results of the multi position rotation error excitation scheme under the small-angle swing base are shown in Fig. 3 and the IMU output data can be seen in Fig. 4. The trajectory simulation results show that while the speed on each axis is always 0 m/s, the angles change according to the

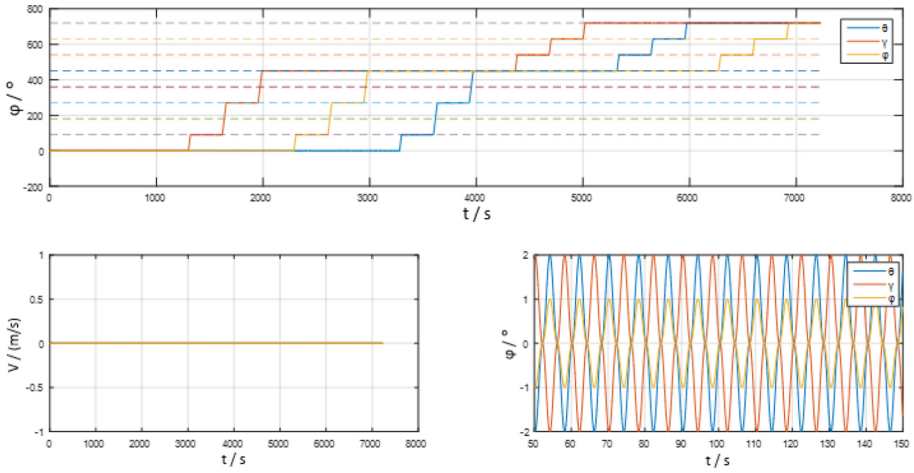

Fig. 3. The trajectory simulation results. The upper figure shows the attitude changes of the trajectory simulation. The bottom-left figure shows the speed changes. The bottom-right figure shows the attitude changes in 50 s–150 s.

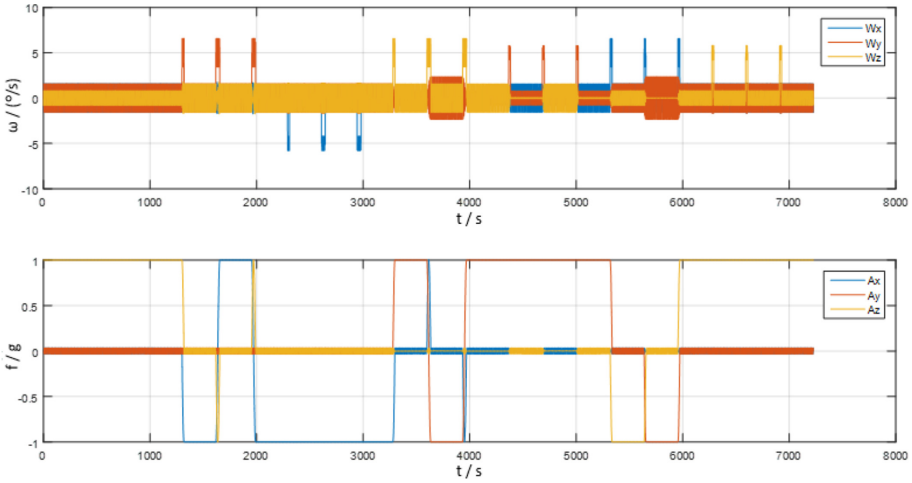

Fig. 4. The simulated IMU output data. The upper figure is the output data of three laser gyroscopes. The bottom figure is the output data of three accelerometers.

Table 1. The comparison of simulation calibration results and preset error parameters.

Parameter	Preset value	Under static base		Under small-angle swing base	
		Estimated value	Relative error (%)	Estimated value	Relative error (%)
B_{gi} (°/h)	0.03 0.05 0.04	0.029991 0.049910 0.039999	−0.0300 −0.1800 −0.0025	0.029995 0.049968 0.039994	−0.0167 −0.0640 −0.0150
K_{gi} (ppm)	150 100 200	149.967 100.055 199.979	−0.0220 0.0550 −0.0105	149.965 100.041 199.980	−0.0233 0.0410 −0.0100
M_{gij} (″)	50/−50 50/−50 50/−50	49.959/−49.965 49.957/−49.983 49.946/−49.974	−0.082/−0.070 −0.086/−0.034 −0.108/−0.052	49.961/−49.966 49.957/−49.985 49.945/−49.973	−0.078/−0.068 −0.086/−0.030 −0.110/−0.054
B_{ai} (ug)	150 100 200	149.990 100.038 199.914	−0.0067 0.0380 −0.0430	149.993 100.043 199.918	−0.0047 0.0430 −0.0410
K_{ai} (ppm)	100 150 200	100.014 150.018 200.000	0.014 0.012 0.000	100.003 150.017 200.007	0.003 0.011 0.004
M_{aij} (″)	−100 100 −100	−99.9678 99.9102 −99.9532	−0.032 −0.090 −0.047	−99.9701 99.9113 −99.9532	−0.030 −0.089 −0.047
D_{ai} (10^{-6} s^2/m)	20 15 25	19.9978 14.9912 24.9779	−0.0110 −0.0587 − 0.0884	19.9825 14.9945 24.9802	− 0.0875 − 0.0367 − 0.0792

preset multi position rotation error excitation scheme and based on this condition, the small-angle swings are added, of which the periods on each axis are 8 s and, except for the heading angle amplitude of 1°, the amplitudes of the other two are both 2°.

The comparison results between the calibration estimated value and the preset error value under both static and small-angle swing bases using systematic calibration method are shown in Table 1. In Table 1, the results show that the calibration accuracy of each error parameter under these two cases is basically the same. Under both static and small-angle swing bases, the relative errors of the simulation calibration experiment results basically do not exceed $\pm$ 0.1%. It can be seen that the systematic calibration method used in this article has a high-precision calibration effect.

The RLG SINS navigation results using this systematic calibration method to compensate the errors are shown in Fig. 5. The calibration and error compensation make the speed errors and the attitude errors not increase significantly with the IMU rotation movement and the increase of time. The navigation errors gradually stabilize during the IMU movement. After the error compensation, the calculation results of the attitudes and the speeds also improve to a certain extent. Therefore, this systematic calibration method has a good compensation performance and is of great significance to the inertial navigation.

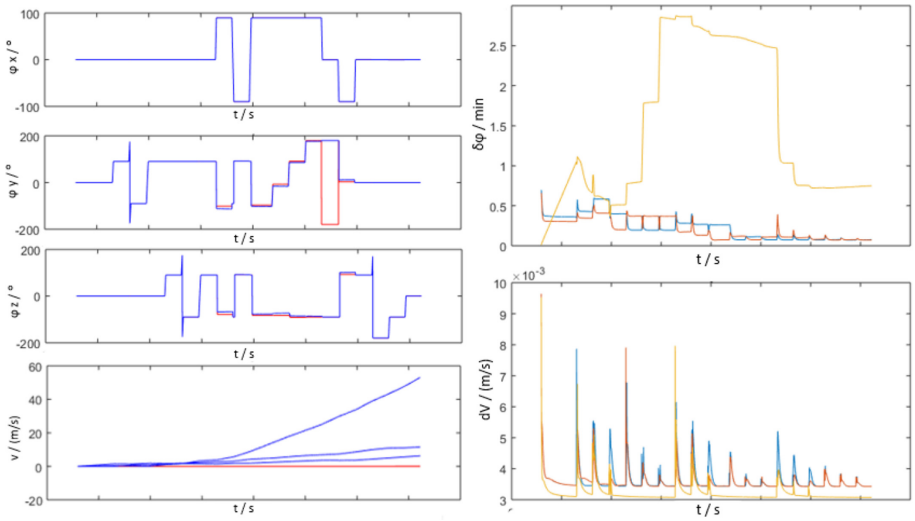

Fig. 5. The RLG SINS navigation results. The first three figures on the left are the navigation results of the attitudes. The fourth figure on the left is the navigation result of the speeds in three axes. In these four pictures, the results after error compensation are red, while the results before correction are blue. Two figures on the right show the changes of the attitude errors and the velocity errors in three axes during filtering process respectively.

5 Conclusion

In this paper, a systematic calibration method for RLG SINS under both static and small-angle swing bases is developed. The calibration simulation experiments are performed under both static and small-angle swing bases. The simulation experiment results show that the calibration accuracy under both of the two cases is basically the same and the relative errors of the simulation calibration experiment results of each error parameter basically do not exceed $\pm$ 0.1%. Besides, the compensation of calibration error parameters also improves the navigation accuracy in the simulation experiments. Therefore, the validity of this high-precision systematic calibration and error estimation method of RLG SINS is verified. This high-precision calibration method not only broadens the environment requirements of calibration, but also has a certain reference value in online calibration applications under the ship mooring state and the missile launcher swing state. In future applications, the requirements for the timeliness of data processing required for online calibration should be emphatically studied.

References

1. Tazartes, D.: An historical perspective on inertial navigation systems. In: 2014 International Symposium on Inertial Sensors and Systems, ISISS. IEEE, Laguna Beach (2014)
2. Nieminen, T., Kangas, J., Suuriniemi, S., et al.: An enhanced multi-position calibration method for consumer-grade inertial measurement units applied and tested. Meas. Sci. Technol. **21**(10), 105204 (2010)
3. Gao, P., Li, K., Wang, L., et al.: A self-calibration method for accelerometer nonlinearity errors in triaxis rotational inertial navigation system. IEEE Trans. Instrum. Meas. **66**(2), 243–253 (2017)
4. Cai, Q., Yang, G., Song, N., et al.: Online calibration of the geographic-frame-equivalent gyro bias in dual-axis RINS. IEEE Trans. Instrum. Meas. **67**(7), 1609–1616 (2018)
5. Li, K., Chen, Y., Wang, L.: Online self-calibration research of single-axis rotational inertial navigation system. Measurement **129**, 633–641 (2018)
6. Gao, P., Li, K., Song, T., et al.: An accelerometers-size-effect self-calibration method for triaxis rotational inertial navigation system. IEEE Trans. Industr. Electron. **65**(2), 1655–1664 (2018)
7. Glueck, M., Oshinubi, D., Manoli, Y.: Automatic real-time offset calibration of gyroscopes. Microsyst. Technol. **21**(2), 429–443 (2014). https://doi.org/10.1007/s00542-014-2115-x
8. Shi, W., Wang, X., Zheng, J., et al.: Multi-position systematic calibration method for RLG-SINS. Infrared Laser Eng. **45**(11), 92–99 (2016)
9. Dranitsyna, E.V.: IMU calibration using sins navigation solution: selection of the rate table motion scenario. In: 2017 24th Saint Petersburg International Conference on Integrated Navigation Systems, ICINS, pp. 1–5. IEEE, St. Petersburg (2017)
10. Wang, Q., Wang, L., Qin, W., et al.: Continuous self-calibration path optimization design of inertial platform based on local observability analysis. J. Chin. Inertial Technol. **26**(6), 713–720 (2018)
11. Cheng, J., Fang, J., Wu, W., et al.: Integrated calibration method for RLG IMU. J. Chin. Inertial Technol. **4**, 445–452 (2014)
12. Jiang, P., Liang, H., Li, H.: Online calibration method of gyro constant drift for low-cost integrated navigator. In: 2019 5th International Conference on Control, Automation and Robotics, ICCAR 2019, pp. 846–850. IEEE (2019)

13. Ma, L., Chen, W., Li, B., et al.: Fast field calibration of MIMU based on the Powell algorithm. Sensors **14**(9), 16062–16081 (2014)
14. Qin, C., Chen, J., Han, Y., et al.: Online calibration method based on dual-axis rotation-modulating laser gyro SINS. In: Proceedings of the 28th Chinese Control and Decision Conference 2016, CCDC, pp. 3311–3315. IEEE, Yinchuan (2016)
15. Jiachong, C., Fei, Y., Ya, Z., et al.: A swing online calibration method of ship-based FOG-IMU. In: 2017 Forum on Cooperative Positioning and Service, CPGPS 2017, pp. 33–38. IEEE (2017)
16. Wang, Z., Shi, Z., Quan, Z.: Online calibration program of SINS for rocket. Infrared Laser Eng. **1**, 266–272 (2015)
17. Wang, H., Shi, Z., Li, G., et al.: Research on simple online calibration scheme of missile SINS. J. Gun Launch Control **39**(4), 6–15 (2018)